Electronic Supplementary Material (ESI) for Journal of Materials Chemistry B.
This journal is © The Royal Society of Chemistry 2023

Supplementary information

Crosslinked albumin-manganese nanoaggregates with sensitized T_1 relaxivity and indocyanine green loading for multimodal imaging and cancer phototherapy

Ying An,[a] Weiwei Chen,[b] Yiran Li,[a] Hongxia Zhao,[a] Deju Ye,[a] Huipu Liu,[a] Kun Wu [a] and Huangxian Ju*,[a]

[a] *State Key Laboratory of Analytical Chemistry for Life Science, School of Chemistry and Chemical Engineering, Nanjing University, Nanjing 210023, China*

[b] *School of Geographic and Biologic Information, Nanjing University of Posts and Telecommunications, Nanjing 210023, China*

* Corresponding author: *E-mail*: hxju@nju.edu.cn (H. X. Ju)

Table of contents

1. Chemicals, reagents and apparatus

Bovine serum albumin (BSA) and propidium iodide (PI) were purchased from Sigma-Aldrich. $KMnO_4$ (analytical reagent, 99.5%) was obtained from Nanjing Chemical Reagent Co., Ltd. Glutaraldehyde (50% in water) was purchased from Energy Chemical (Shanghai). Indocyanine green (ICG) was obtained from Shanghai Aladdin Biochemical Technology Co., Ltd. 1,3-diphenylisobenzofuran (DPBF) was obtained from Shanghai Bide Pharmaceutical Technology Co., Ltd. Fine bore polythene tube (0.86 mm i.d., 1.27 mm o.d.) was purchased from Smiths Medical (USA). TM-100 ultrasound gel was purchased from Tianjin Jinya Technology Development Co., Ltd. Cell Counting Kit-8 (CCK-8) was purchased from Sangon Biotech Co., Ltd (Shanghai). Hoechst 33342 was purchased from Thermo Fisher Scientific. Roswell Park Memorial Institute 1640 medium (RPMI-1640), phosphate buffered saline (PBS), trypsin, 2′,7′-dichlorofluorescein diacetate (DCFH-DA), Calcein AM, Lyso-Tracker Green and Annexin V-FITC/PI cell apoptosis kits were obtained from KeyGen Biotech. Co. Ltd (Nanjing). Fetal bovine serum (FBS) was obtained from Longtimebio Technology Co., Ltd (Nanjing). 4% paraformaldehyde solution was purchased from Beyotime Biotechnology. Deionized (DI) water (18.4 MΩ) used in all experiments was produced by Millipore Elix 5 water purification system.

TEM images, scanning transmission electron microscopy dark field (STEM-DF) and energy dispersive spectroscopic (EDS) elemental mapping were captured on JEM-2800 transmission electron microscope (JEOL Ltd., Japan) and FEI Tecnai F20 transmission electron microscope (USA). Mn content analysis was performed with Avio500 inductively coupled plasma atomic emission spectrometer (ICP-AES, PE, USA). Elemental analysis was conducted on PHI5000 VersaProbe X-ray photoelectron spectrometer (XPS, ULVAC-PHI, Japan). Fourier transform infrared spectra (FT-IR) were recorded with Nicolet iS50 FT-IR spectrometer (Thermo Fisher Scientific). Circular dichroism (CD) spectra were obtained with Applied Photophysis Chirascan (Applied Photophysis, UK). Dynamic light scattering (DLS) analysis was conducted on BI-200SM wide angle dynamic and static laser light scatterer (Brookhaven, USA, laser wavelength: 663 nm). Zeta potential analysis was conducted on Nano-Z Zetasizer (Malvern, UK). UV-vis-NIR absorption spectra were recorded with UV-3600 spectrophotometer (Shimadzu, Japan). MR relaxivity was measured on a 0.5 T MR scanner (NMI20-015 V-I, NIUMAG). NIR fluorescence spectra were obtained with FLS980 fluorescence spectrometer (Edinburgh, UK). CCK-8 assay was performed on a Multiskan FC microplate reader (Thermo Fisher Scientific). Fluorescence images of cells were acquired with a Leica TCS SP8 confocal laser scanning microscope. Flow cytometric analysis was conducted on Cytoflex S flow cytometer (Beckman Coulter, USA). All MR imaging experiments

were performed on a 1.0 T small animal MR scanner (Bruker ICON™). In vitro or in vivo NIR-II fluorescence imaging was carried out with NIR-II in vivo imaging system (Series III 900/1700, Suzhou NIR-Optics Technologies Co., Ltd., China). All PA imaging experiments were accomplished with Vevo LAZR 2100 imaging system (FUJIFILM VisualSonics, Canada). Photothermal images were recorded by an IR thermal camera (Fotric 225-1, Fotric, China).

2. *In vitro* PA imaging

In vitro PA imaging experiments were carried out with the Vevo LAZR 2100 imaging system. C-BM/I or ICG solution was injected into a fine bore polythene tube, then the tube was sunk into the bottom of a transparent box filled with ultrasound gel. Subsequently, the box was placed on the sample stage of the PA imaging system and scanned with the LZ-250 detector to acquire the PA spectra (680-970 nm) or the PA intensities at 830 nm.

3. Evaluation of photothermal conversion efficiency

To measure the photothermal conversion efficiency (η), 280 μL C-BM/I solution (16 μg/mL [ICG]) or ICG solution (16 μg/mL) in Eppendorf tube was irradiated with 808 nm laser (0.33 W/cm^2) followed by natural cooling to room temperature after reaching the maximum temperature. The η is calculated according to the method reported previously: [S1-S4]

$$\eta = \frac{hS(T_{max} - T_{surr}) - Q_{dis}}{I(1 - 10^{-A_\lambda})} \times 100\% \quad (1)$$

where h is the heat transfer coefficient, S is the surface area of the sample well. hS can be determined by applying the linear time data from the cooling period vs lnθ:

$$hS = \frac{m\, C_{H_2O}}{\tau_s} \quad (2)$$

m is the mass of the sample solution (0.28 g), and its heat capacity value (C_{H2O}) is approximated to be 4.2 J/(g·°C). The slope of the linear equation (τ_s) of C-BM/I vs ICG in Fig. S16b and Fig. S16d is 162.04 s and 161.97 s, respectively. τ_s is the associated time constant:

$$t = -\tau_s \ln\theta \quad (3)$$

θ is a dimensionless parameter, known as the driving force temperature:

$$\theta = \frac{T - T_{surr}}{T_{max} - T_{surr}} \quad (4)$$

T_{max} is the maximum temperature, which is 48.4 °C for C-BM/I (Fig. S16a) and 45.8 °C for ICG in (Fig. S16c). T_{surr} is the ambient temperature (26.1 °C).

Q_{dis} is the heat energy of the quartz cell and solvent without nanoparticles, and can be calculated according to the following equation:

$$Q_{dis} = \frac{m' C_{H2O}(T'_{max} - T_{surr})}{\tau'_s} \quad (5)$$

m' is the mass of deionized water (0.28 g). C_{H2O} is the heat capacity, which is approximated to be 4.2 J/(g·°C). T'_{max} is the maximum temperature in Fig. S16e (29.7 °C). T_{surr} is the ambient temperature (26.1 °C). The slope of the linear equation (τ's) in Fig. S16f is173.52 s. Therefore, Q_{dis} is calculated to be 24.4 mW.

I is the laser power (I = 0.33 W/cm^2 × π × (1 cm)^2 = 0.33π W). A_{808} is the absorbance of C-BM/I and ICG at 808 nm, which is 0.756 and 0.694, respectively. Finally, the η of C-BM/I and ICG can be calculated according to Equation (1), which is 16.0% and 14.3%, respectively.

4. Cell culture and cellular uptake of C-BM/I

Human non-small cell NCI-H460 lung cancer cells were purchased from KeyGen Biotech. Co. Ltd and cultured in RPMI-1640 supplemented with 10% (v/v) FBS and 1% penicillin/streptomycin in a humidified atmosphere containing 5% CO_2 at 37 °C. The cells were counted by Countess II automated cell counter (Thermo Fisher Scientific).

After H460 cells (~2 × 10^4 cells/well) were seeded on a glass-bottom dish (In Vitro Scientific, D35C4-20-1-N) by above culture procedure overnight, the cells were incubated with 150 μL fresh medium containing C-BM/I (10 μg/mL [ICG]) for 1, 2, 4 and 6 h to observe the confocal FL images with excitation at 665 nm and emission from 675 to 795 nm after replacing the medium with PBS.

5. Colocalization imaging

To examine the intracellular location of C-BM or C-BM/I, C-BM/I and H460 cells were used for colocalization experiments. The cells were firstly incubated with C-BM/I (10 μg/mL [ICG]) for 4 h. After removing the medium, the cells were further stained with Hoechst 33342 (5 μg/mL) for 10 min followed with Lyso-Tracker Green (200 nM) for 10 min to acquire the FL images on SP8 confocal laser scanning microscope with excitation at 405 nm (430-500 nm emission), 488 nm (498-540 nm emission) and 665 nm (675-795 nm emission), respectively.

6. *In vitro* singlet oxygen generation

0.8 mL C-BM/I or ICG dispersed ethanol solution (5 μg/mL [ICG]) was mixed with 10 μL DPBF ethanol solution (2 mg/mL), and irradiated with 808 nm laser (0.33 W/cm^2) for 0-5 min. The DPBF

ethanol solution without C-BM/I or ICG was used as blank control. DPBF absorption was monitored from 350 to 455 nm and the relative absorbance (%) was calculated at 412 nm.

The intracellular singlet oxygen generation was measured by incubating H460 cells with C-BM/I or ICG (40 μg/mL [ICG]) for 4 h, and 50 μM DCFH-DA diacetate for 30 min at 37 °C. The treated cells were then exposed under 808 nm laser (0.77 W/cm^2) for 5 min to take the fluorescence images with excitation at 488 nm. Control experiments without 808 nm laser irradiation or probe incubation were also performed.

7. Cytotoxicity detected with CCK-8

The cytotoxicity of C-BM/I or ICG with or without laser irradiation was assessed by CCK-8 assay. After H460 cells were seeded in 96-well cell culture plates at a density of 1 × 10^4 cells/well by above culture procedure, the cells were incubated with C-BM/I or ICG at different concentrations (0, 2, 4, 6, 8, 10 μg/mL [ICG]) for 4 h. Part of the plates were irradiated with 808 nm laser (0.77 W/cm^2) for 5 min, and then the cells were kept growing for another 12 h at 37 °C to examine the light toxicity. The others were kept incubation for another 12 h to determine the dark toxicity. The toxicity was detected by adding fresh medium (100 μL) and CCK-8 (10 μL) in each well in sequence to incubate for another 3 h and then record the absorbance (OD) at 450 nm. The percentage of cell viability was calculated as $[(A_s\text{-}A_b)/(A_c\text{-}A_b)] \times 100$, where A_s referred to the absorbance of cells with probes, A_c referred to the absorbance of cells without probes, and A_b referred to the absorbance of medium and CCK-8 solution.

8. Cell viability detected with Calcein AM/PI staining

Calcein AM/PI staining experiments were implemented to identify the viability of C-BM/I or ICG treated cells before or after laser irradiation. H460 cells (~1 × 10^5) were seeded on a glass-bottom dish (In Vitro Scientific, D35-20-1-N) by above culture procedure, and then incubated with C-BM/I or ICG (6 μg/mL [ICG]) for 4 h. Subsequently, the cells were treated with or without laser irradiation for 5 min (808 nm, 0.77 W/cm^2) and then incubated for another 6 h at 37 °C. Afterward, the cells were rinsed, and 0.5 mL of the mixture of Calcein AM (2 μM) and PI (8 μM) was added into each dish to incubate for another 30 min. After removal of the medium, the cells were washed carefully with PBS for three times, trypsinized and resuspended in PBS for FL imaging with SP8 confocal laser scanning microscope. The fluorescence from Calcein AM and PI was collected at green channel (505-540 nm) with excitation at 495 nm and red channel (565-620 nm) with excitation at 552 nm, respectively.

9. Flow cytometric analysis

After H460 cells (~2 × 10^5 cells/well) were seeded in 6-well plates by above culture procedure, and incubated with 2 mL fresh medium containing C-BM/I or ICG (6 μg/mL [ICG]) for 4 h, the cells were irradiated with or without 808 nm laser (0.77 W/cm^2) for 5 min and then incubated for another 6 h. Afterward, the cells were trypsinized, washed with PBS for three times, and resuspended in 400 μL binding buffer for flow cytometric analysis by incubating them with the mixture of Annexin V-FITC (4 μL) and PI (4 μL) for 10 min in the dark.

10. Animals and tumor models

Pathogen-free BALB/c female nude mice (5-6 weeks) were purchased from Shanghai Lingchang Biotechnology Co., Ltd. (Shanghai, China). The Institutional Animal Care and Use Committee (IACUC) of Nanjing University approved and provided guidance on this study protocol (Approval No: IACUC-2208003). To establish subcutaneous (s.c.) tumor, H460 cells (3.0 × 10^6) were suspended in 50 μL complete medium containing 50% (v/v) matrigel, and then injected subcutaneously into the axilla position of right forelimb of mouse. After the tumor reached 7-8 mm in a single aspect, the tumor-bearing mice were used for NIR-II FL imaging, T_1-weighted MR imaging, PA imaging and photothermal therapy.

11. *In vivo* photothermal-photodynamic therapy and histopathological analysis

H460 tumor-bearing nude mice were i.t. injected with 50 μL saline, ICG or C-BM/I (80 μg/mL [ICG]). After injection for 2 h, the temperature of C-BM/I or ICG-treated tumor tissue during irradiation of 808-nm laser (0.55 W/cm^2) for 5 min was monitored by infrared thermal imaging.

For photothermal-photodynamic therapy, H460 tumor-bearing mice were weighted and randomly divided into six groups: (1) saline only, (2) saline plus laser irradiation, (3) ICG only, (4) ICG plus laser irradiation, (5) C-BM/I only, and (6) C-BM/I plus laser irradiation. Groups (1) and (2) were i.t. injected with 50 μL saline, groups (3) and (4) were injected with 50 μL ICG (80 μg/mL), and groups (5) and (6) were injected with 50 μL C-BM/I (80 μg/mL [ICG]). After injection for 2 h, groups (2), (4) and (6) were irradiated with 808-nm laser (0.55 W/cm^2) for 5 min. The injection and irradiation procedures were repeated at day 3 and day 7. The tumor size and body weight of each mouse were measured with a digital vernier caliper and an electronic balance every two days. The tumor volumes were calculated as $V = (L \times W^2)/2$, where L and W represents the length and width of the tumor respectively.

At day 14, all mice were sacrificed, and representative photos of mice from different groups were taken. For histopathological analysis, the tumor tissues of mice were excised, washed with PBS and fixed in 4% paraformaldehyde solution. Afterwards, the tumors were embedded in paraffin, sectioned and stained with the H&E or TUNEL staining kit to acquire the images. Besides, major organs of the mice in group (1) and group (6) were excised for H&E staining analysis to examine the potential biological toxicity.

12. Supplementary figures

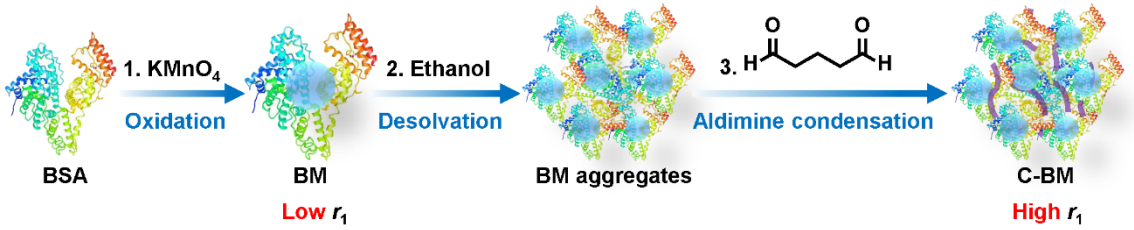

Fig. S1 Schematic diagram of the preparation process of crosslinked C-BM nanoaggregates.

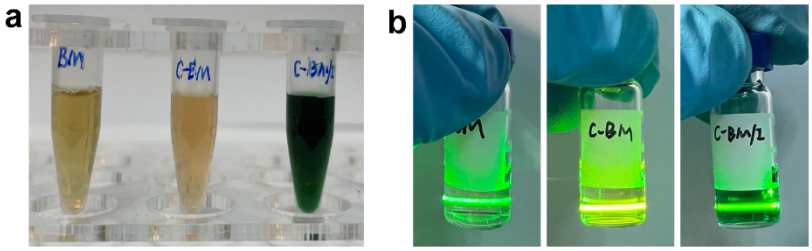

Fig. S2 (a) Photographs and (b) Tyndall effect of obtained BM (left), C-BM (middle) and C-BM/I (right) solution.

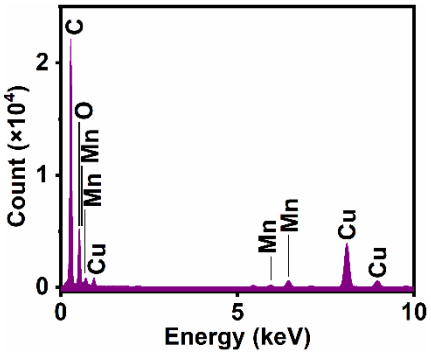

Fig. S3 EDS spectrum of C-BM in Fig. 1c.

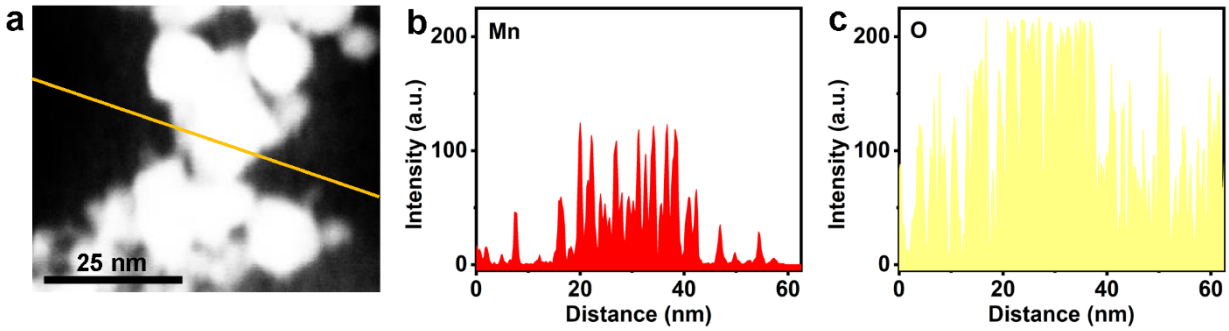

Fig. S4 (a) TEM of C-BM. (b,c) Corresponding EDS line profiles showing the distribution of (b) Mn element and (c) O element in (a).

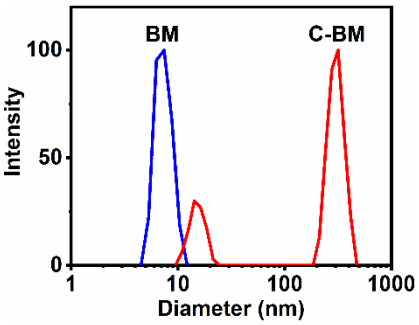

Fig. S5 Dynamic light scattering (DLS) analysis of BM and C-BM.

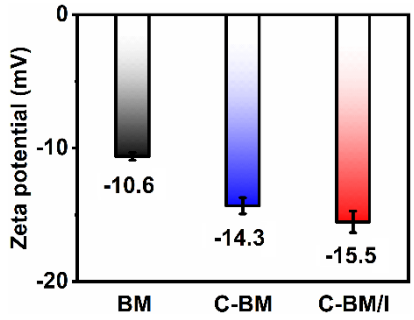

Fig. S6 Zeta potential analysis of BM, C-BM and C-BM/I. Error bars represent standard deviation (SD, $n = 3$).

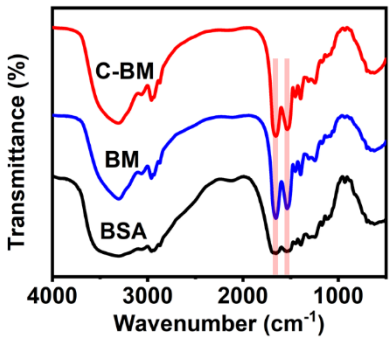

Fig. S7 FT-IR spectra of BSA, BM and C-BM.

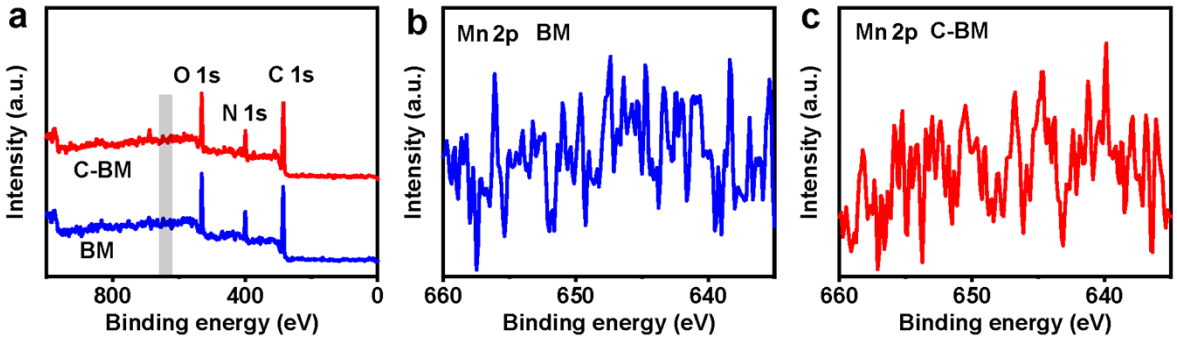

Fig. S8 (a) XPS spectra of BM and C-BM. Mn 2p spectra of (b) BM and (c) C-BM.

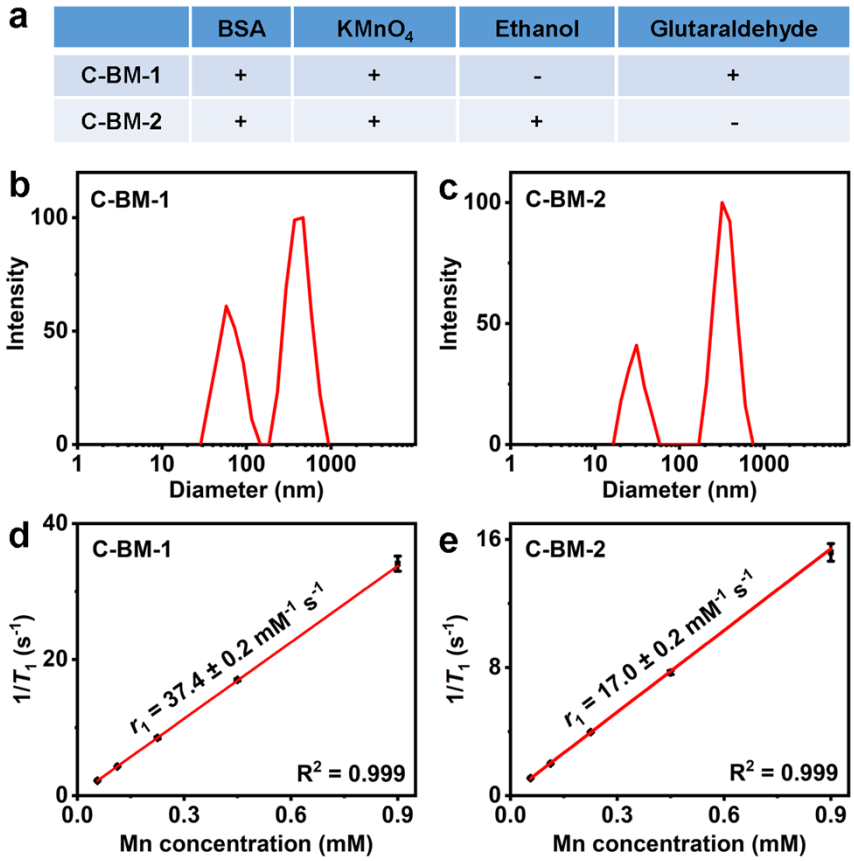

Fig. S9 (a) Synthesis of control C-BM-1 and C-BM-2. (b,c) DLS analysis of (b) C-BM-1 and (c) C-BM-2. (d,e) Plots of $1/T_1$ of (d) C-BM-1 and (e) C-BM-2 at 0.5 T versus Mn concentration in the solution. Error bars represent SD (n = 3).

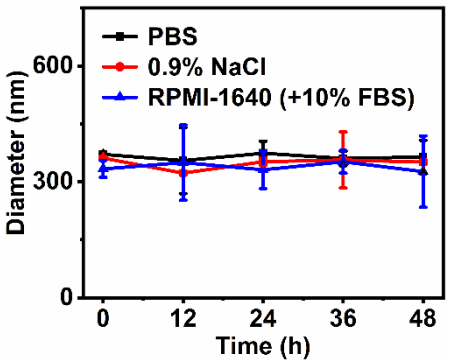

Fig. S10 Stability of DLS diameter at 100% intensity of C-BM in PBS, 0.9% NaCl or RPMI-1640 medium containing 10% FBS at 4 °C. Error bars represent SD (n = 3).

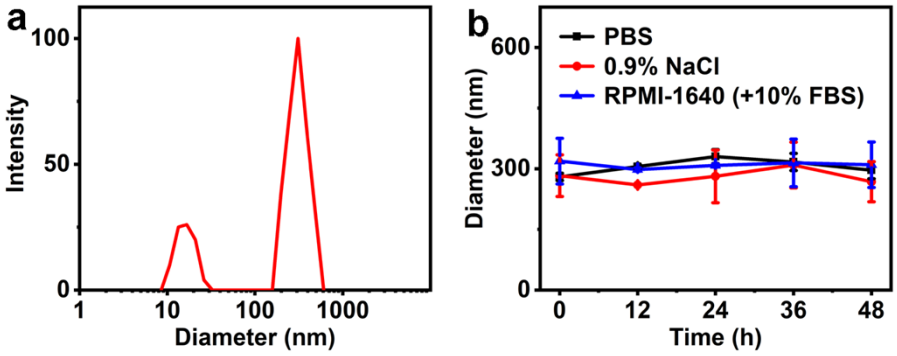

Fig. S11 (a) DLS analysis of C-BM/I. (b) Stability of DLS diameter at 100% intensity of C-BM/I in PBS, 0.9% NaCl or RPMI-1640 medium containing 10% FBS at 4 °C. Error bars represent SD (n = 3).

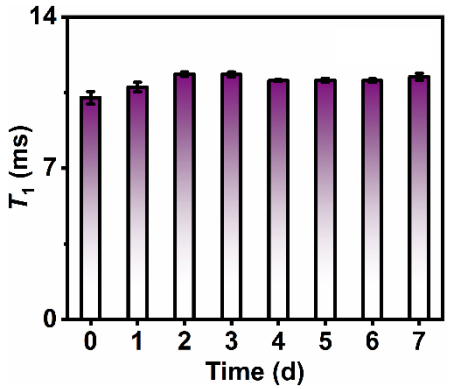

Fig. S12 Stability of T_1 relaxation time of protons in C-BM/I solution (0.9 mM [Mn]) at 0.5 T during storage at 4 °C for 0 to 7 days. Error bars represent SD (n = 3).

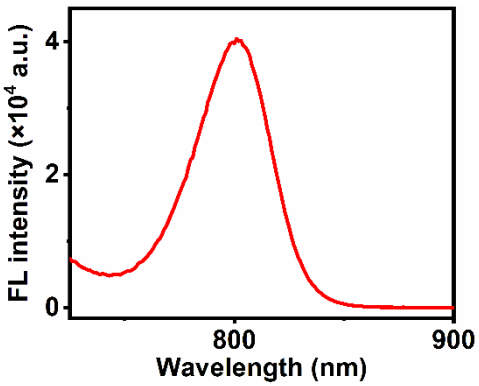

Fig. S13 NIR-I fluorescence spectrum of C-BM/I solution (12.5 μg/mL [ICG]) with 665-nm excitation.

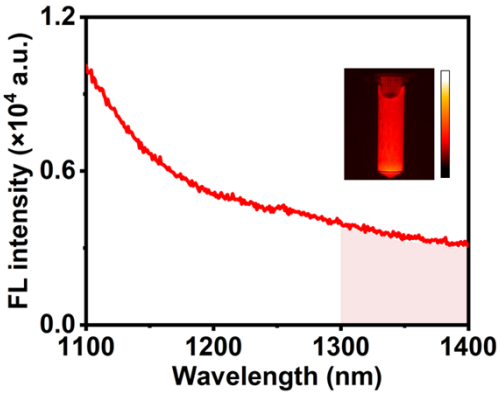

Fig. S14 NIR-II fluorescence spectrum of C-BM/I solution (12.5 μg/mL [ICG]) with 808-nm excitation under 1100-nm LP filter. Inset: NIR-II FL image with 808-nm excitation (10 W), 150-ms exposure time and 1300-nm LP filter.

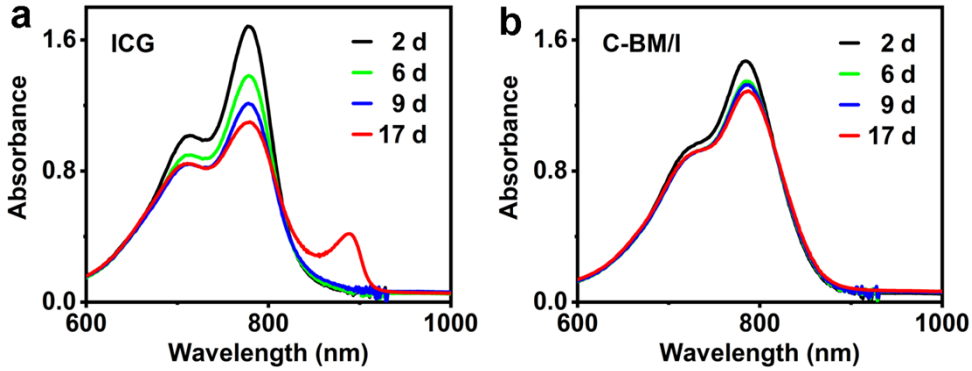

Fig. S15 Vis-NIR absorption spectra of (a) ICG and (b) C-BM/I solution (10 μg/mL [ICG]) after storage at 4 °C for 2, 6, 9 and 17 days.

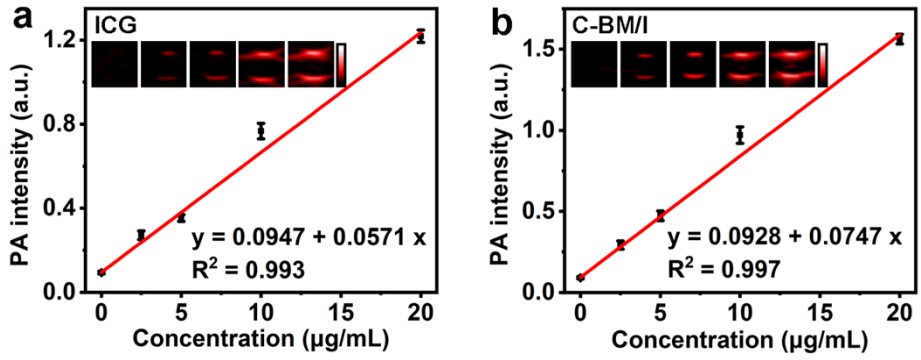

Fig. S16 Plots of PA intensity of (a) ICG and (b) C-BM/I solution at 830-nm excitation versus ICG concentration. Inset: Corresponding PA images. Error bars represent SD (n = 3).

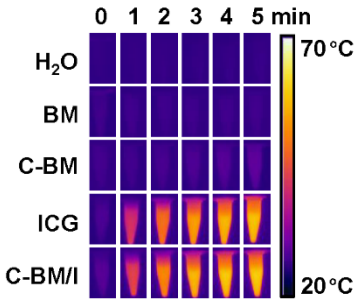

Fig. S17 Corresponding photothermal images in Fig. 2h.

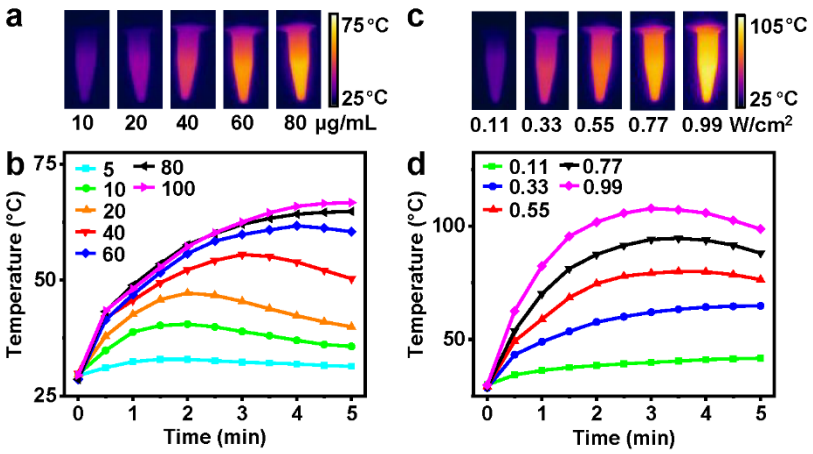

Fig. S18 Photothermal images and time-dependent temperature of C-BM/I at (a,b) marked ICG concentrations (μg/mL) under 0.33 W/cm^2 and (c,d) marked power densities (W/cm^2) at 80 μg/mL ICG concentration under 808-nm laser irradiation.

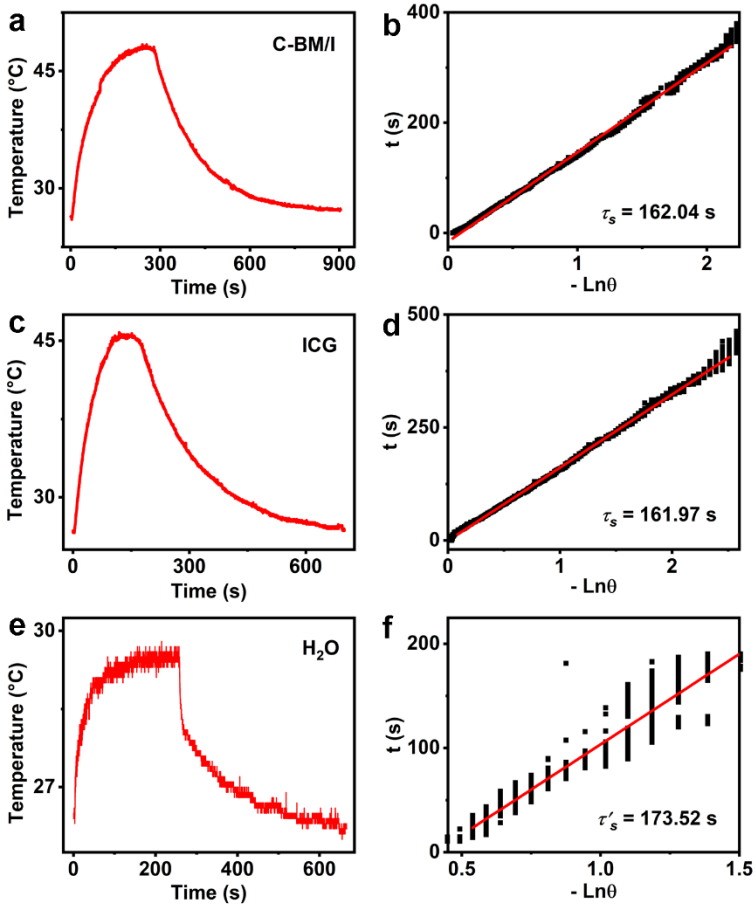

Fig. S19 Photothermal effect of (a) C-BM/I (16 μg/mL [ICG]), (c) ICG (16 μg/mL) and (e) H_2O under 808 nm laser (0.33 W/cm^2), which was turned off after reaching its maximum temperature. (b,d,f) Linear time data vs -lnθ obtained from a, c and e. The η of C-BM/I and ICG was calculated to be 16.0% and 14.3%, respectively.

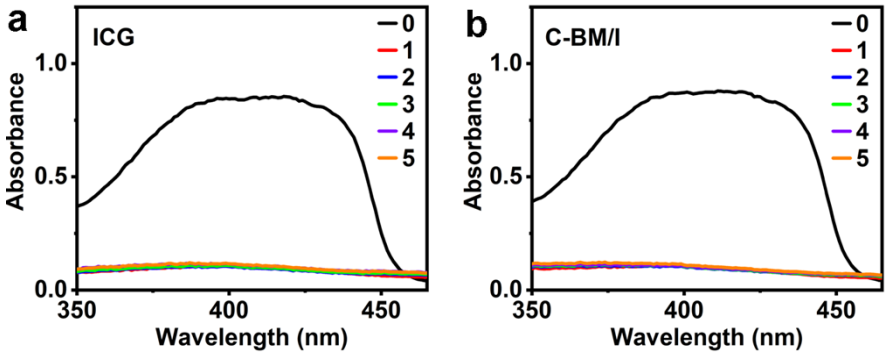

Fig. S20 UV-Vis absorption spectra of DPBF ethanol solution incubated with (a) ICG and (b) C-BM/I ethanol solution (5 μg/mL [ICG]) under 808 nm laser irradiation (0.33W/cm^2) for 0-5 min.

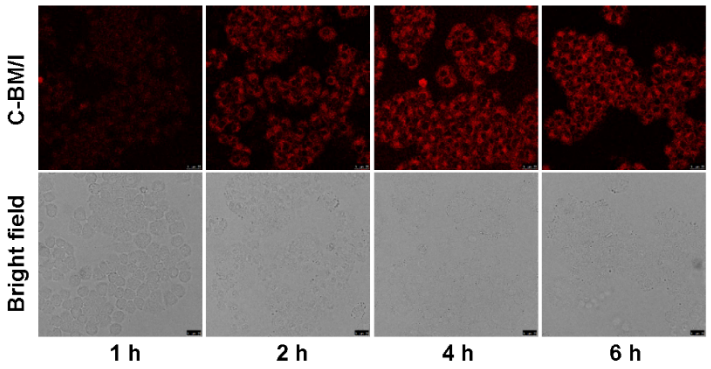

Fig. S21 Fluorescence images of H460 cells following incubation with C-BM/I (10 μg/mL [ICG]) for 1, 2, 4 and 6 hours. Scale bar: 25 μm.

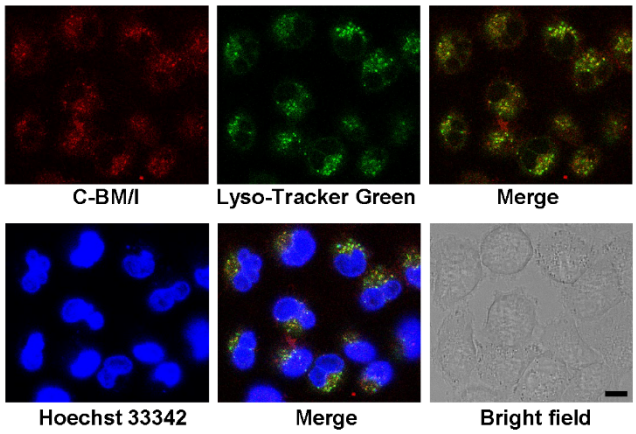

Fig. S22 Colocalization analysis of H460 cells after incubation with C-BM/I (10 μg/mL [ICG]) and co-staining with Lyso-Tracker Green (200 nM) and Hoechst 33342 (5 μg/mL). Scale bar: 10 μm.

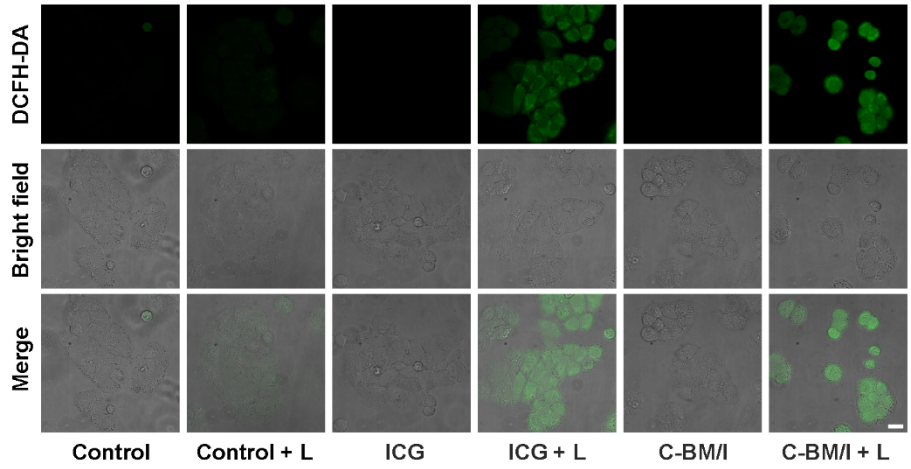

Fig. S23 Fluorescence images of C-BM/I or ICG (40 μg/mL [ICG]) treated H460 cells before and after laser irradiation (808 nm, 0.77 W/cm^2) for 5 min, and then staining with DCFH-DA. The cells without C-BM/I or ICG treatment were used as control. Scale bar: 20 μm.

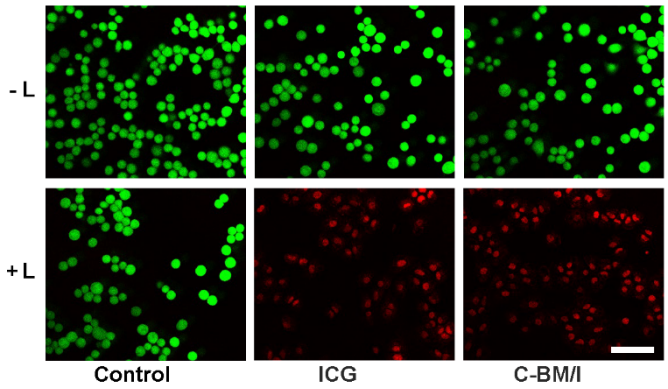

Fig. S24 Fluorescence images of C-BM/I or ICG (6 μg/mL [ICG]) treated H460 cells before (-L) and after (+L) laser irradiation (808 nm, 0.77 W/cm^2) for 5 min, and then co-staining with Calcein AM (live cells, green) and PI (dead cells, red). The cells without C-BM/I or ICG treatment were used as control. Scale bar: 75 μm.

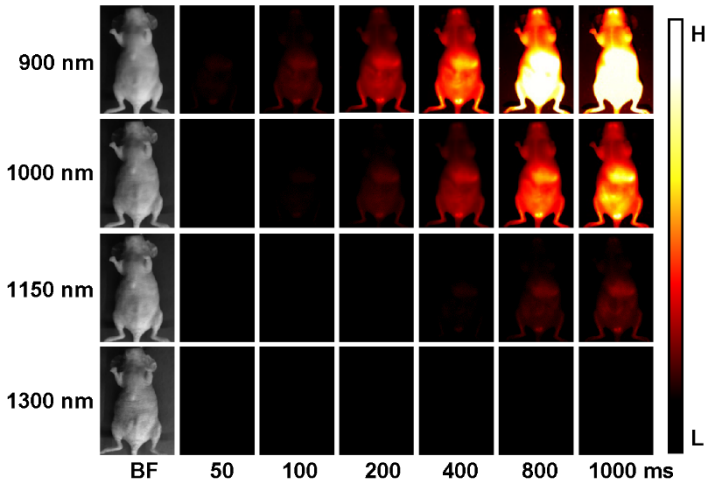

Fig. S25 NIR-II fluorescence images of healthy mice without any treatment under 900-, 1000-, 1150- and 1300-nm LP filters with the exposure times of 50, 100, 200, 400, 800 and 1000 ms at 808-nm excitation (10 W). BF = bright field.

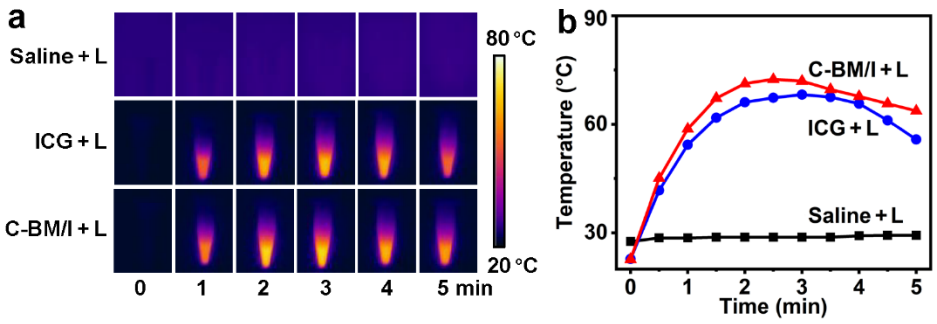

Fig. S26 (a) Photothemal images and (b) time-dependent temperature of 50 μL normal saline, ICG (80 μg/mL) and C-BM/I (80 μg/mL [ICG]) saline solution under 808-nm laser irradiation (0.55 W/cm^2). L = laser.

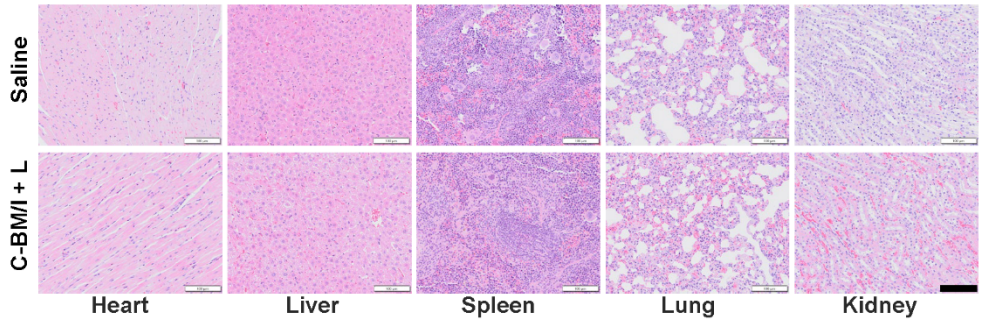

Fig. S27 Representative H&E staining images of major mouse organs including heart, liver, spleen, lung and kidney resected from group (1) and group (6) at day 14. L = laser. Scale bar: 100 μm.

13. Supplementary tables

Table S1 Comparison of T_1 relaxivity (r_1) of albumin-manganese-based nanocomposites (AMNs) with different sizes and ratios of Mn:A at different magnetic flux densities (MFD).

AMN	Size [nm][a]	Ratio of [Mn:A][b]	Mn content[c]	r_1 [mM^{-1} s^{-1}]	MFD	Ref
BM	7.4	5.6	0.34%	5.49	0.5 T	This work
C-BM	317	**5.6**	**0.35%**	**67.2**	0.5 T	This work
C-BM/I	309	5.6	N.D.[d]	**97.3**	0.5 T	This work
BM	8.7	53.1	2.8%	7.9	0.5 T	S5
BMP	10.1	53.1	0.9%	13.9	0.5 T	S5
BMI	11.7	53.1	1.2%	70.6	0.5 T	S5
BM	8.9	53.1	3.76%	5.9	0.5 T	S6
OMPN	90.4	42.2	2.6%	31.07	0.52 T	S7
PMHN-DA	60.85	63.0	3.0%	38.14	0.52 T	S8
PMHN-PY	7.47	63.0	N.D.	13.15	0.52 T	S8
PMHN-DP	20.97	63.0	N.D.	13.53	0.52 T	S8
PMHN-EGC	6.99	63.0	N.D.	22.41	0.52 T	S8

[a] The size is determined by DLS analysis. [b] Ratio of Mn:A: input molar ratio of Mn element from $KMnO_4$ to albumin (BSA or ovalbumin). [c] The Mn content is determined by ICP-AES or ICP-MS measurement. [d] Not determined.

Table S2 Comparison of T_1 relaxivity (r_1) of manganese oxide (Mn_xO_y) or Mn_xO_y-based nanocomposites with different sizes at different MFD.

Mn_xO_y	**Size [nm][a]**	**r_1 [mM^{-1} s^{-1}]**	**MFD**	**Treatment**	**Ref**
C-BM	~18.8	**67.2**	0.5 T	-[b]	This work
C-BM/I	~18.8	**97.3**	0.5 T	-	This work
MnO	7	0.37	3.0 T	-	S9
	15	0.18	3.0 T		
	20	0.13	3.0 T		
	25	0.12	3.0 T		
MnO	20	0.353	1.5 T	-	S10
hMnO	20	1.150	1.5 T	-	S10
MnO@SiO_2	~100	1.34	3.0 T		S10
		3.34	0.47 T		
MnO	10	0.81	3.0 T	-	S11
MnO	2-3	7.02	1.5 T	-	S12
hMON-m	16 (core)	2.58	7.0 T	-	S13
hMON-s	16 (core)	1.23	7.0 T	-	S13
sMON-m	16 (core)	2.22	7.0 T	-	S13
sMON-s	16 (core)	1.17	7.0 T	-	S13
hmMn_2O_3	300-500	0.17	3.0 T	-	S14
		6.49	3.0 T	H^+/GSH	
Mn_3O_4@SiO_2	100	13.39	3.0 T	-	S15
		25.17	3.0 T	GSH	
Mn_3O_4	9	8.26	3.0 T	-	S16
HMCNs	200-350	0.79	3.0 T	-	S17
		8.81	3.0 T	H^+	
Mn_3O_4	9.8	1.31	3.0 T	-	S18
	10	2.06	3.0 T		
	5	1.08	3.0 T		
WMONs	20	0.21	3.0 T	-	S19
HMONs	20	1.42	3.0 T	-	S19
MnO_2	200	0.007	3.0 T	-	S20
		3.4	3.0 T	H^+ (pH 6)	

		4	3.0 T	H^+ (pH 4.6)	
MnO_2	141	0.1	1.5 T	-	S21
		4.89	1.5 T	GSH	
MS@MnO_2	80-100	0.50	N.D.	-	S22
		6.91	N.D.	GSH	
Ce6@MnO_2-	~ 100	0.78	3.0 T	-	S23
PEG		6.53	3.0 T	H^+	
H-MnO_2-PEG	120-190	0.051	3.0 T	-	S24
		8.743	3.0 T	H^+	
UCMnPt	> 70	0.63	1.2 T	-	S25
		8.65	1.2 T	GSH	
MCIH	100-250	2.20	9.4 T	-	S26
		16.24	9.4 T	H^+	

[a] The size is determined by TEM analysis. [b] No treatment.

Table S3 Comparison of T_1 relaxivity (r_1) change before and after aggregation and crosslinking assembly of BM with those of the Gd^{3+}-based materials reported previously.

Precursor	**r_1 [pre, mM^{-1} s^{-1}][a]**	**r_1 [post, mM^{-1} s^{-1}][b]**	**Increase**	**MFD**	**Ref**
BM	5.49	67.2	**12.2-fold**	0.5 T	This work
1	3.9	8.3	2.1-fold	1.5 T	S27
1-I	19.6	29.8	1.5-fold	0.5 T	S28
	19.4	27.8	1.4-fold	1.5 T	
	16.8	19.0	1.1-fold	3.0 T	
1-II	18.0	29.4	1.6-fold	0.5 T	S28
	17.4	26.8	1.5-fold	1.5 T	
	15.0	18.4	1.2-fold	3.0 T	
1-O	25.0	34.2	1.4-fold	0.5 T	S28
	22.8	31.8	1.4-fold	1.5 T	
	17.6	21.0	1.2-fold	3.0 T	
Probe **1**	10.2	19.0	1.9-fold	1.0 T	S29
	10.2	15.6	1.5-fold	1.5 T	
	9.3	10.3	1.1-fold	3.0 T	
P-CyFF-Gd	8.9	20.1	2.3-fold	0.5 T	S30
1-RGD	N.D.	20.0	N.D.	0.5 T	S31
2-RGD	7.5	20.9	2.8-fold	0.5 T	S31
P-FFGd-TCO	8.33	19.69	2.4-fold	0.5 T	S32

[a] The T_1 relaxivity of BM or Gd^{3+}-based compounds. [b] The T_1 relaxivity of C-BM or the self-assembled Gd^{3+}-based nanoassemblies.

Table S4 Comparison of the photothermal conversion efficiency (PCE) of ICG and ICG-based photothermal agents reported previously under 808 nm laser irradiation.

Photothermal agent	Concentration	Power density	PCE	Ref
C-BM/I	16 μg/mL [ICG]	0.33 W/cm^2	16.0%	This work
ICG	16 μg/mL	0.33 W/cm^2	14.3%	This work
PEG-Hep-ICG PMs	50 μg/mL [ICG]	0.8 W/cm^2	18.2%	S33
PEG-TK-ICG PMs	50 μg/mL [ICG]	0.8 W/cm^2	17.9%	S33
ICG	50 μg/mL	0.8 W/cm^2	16.1%	S33
ICG	5 μg/mL	1 W/cm^2	15.5%	S34
PDA-PEG-ICG-Fe^{3+}	200 μg/mL	2 W/cm^2	26.5%	S35
ICG-Au@BSA-Gd	10 μg/mL [ICG]	1.5 W/cm^2	21.77%	S36

14. Supplementary references

S1 H. Shi, Y. Sun, R. Yan, S. Liu, L. Zhu, S. Liu, Y. Feng, P. Wang, J. He, Z. Zhou and D. Ye, *Nano Lett.*, 2019, **19**, 937-947.

S2 D. Xi, M. Xiao, J. Cao, L. Zhao, N. Xu, S. Long, J. Fan, K. Shao, W. Sun, X. Yan and X. Peng, *Adv. Mater.*, 2020, **32**, 1907855.

S3 S. Li, Q. Deng, Y. Zhang, X. Li, G. Wen, X. Cui, Y. Wan, Y. Huang, J. Chen, Z. Liu, L. Wang and C.-S. Lee, *Adv. Mater.*, 2020, **32**, 2001146.

S4 Y. Sun, H. Shi, X. Cheng, L. Wu, Y. Wang, Z. Zhou, J. He, H.-Y. Chen and D. Ye, *CCS Chem.*, 2020, **2**, 1336-1349.

S5 J. Pan, Y. Wang, H. Pan, C. Zhang, X. Zhang, Y.-Y. Fu, X. Zhang, C. Yu, S.-K. Sun and X.-P. Yan, *Adv. Funct. Mater.*, 2017, **27**, 1603440.

S6 W. Hou, Y. Jiang, G. Xie, L. Zhao, F. Zhao, X. Zhang, S.-K. Sun, C. Yu and J. Pan, *Nanoscale*, 2021, **13**, 8531-8542.

S7 B. Xiao, D. Li, H. Xu, X. Zhou, X. Xu, Y. Qian, F. Yu, H. Hu, Z. Zhou, X. Liu, J. Gao, N. K. H. Slater, Y. Shen and J. Tang, *Biomaterials*, 2021, **274**, 120893.

S8 B. Xiao, X. Zhou, H. Xu, B. Wu, D. Hu, H. Hu, K. Pu, Z. Zhou, X. Liu, J. Tang and Y. Shen, *ACS Nano*, 2018, **12**, 12682-12691.

S9 H. B. Na, J. H. Lee, K. An, Y. I. Park, M. Park, I. S. Lee, D.-H. Nam, S. T. Kim, S.-H. Kim, S.-W. Kim, K.-H. Lim, K.-S. Kim, S.-O. Kim and T. Hyeon, *Angew. Chem., Int. Ed.*, 2007, **46**, 5397-5401.

S10 K. An, S. G. Kwon, M. Park, H. B. Na, S.-I. Baik, J. H. Yu, D. Kim, J. S. Son, Y. W. Kim, I. C. Song, W. K. Moon, H. M. Park and T. Hyeon, *Nano Lett.*, 2008, **8**, 4252-4258.

S11 Y. Lu, L. Zhang, J. Li, Y.-D. Su, Y. Liu, Y.-J. Xu, L. Dong, H.-L. Gao, J. Lin, N. Man, P.-F. Wei, W.-P. Xu, S.-H. Yu and L.-P. Wen, *Adv. Funct. Mater.*, 2013, **23**, 1534-1546.

S12 M. J. Baek, J. Y. Park, W. Xu, K. Kattel, H. G. Kim, E. J. Lee, A. K. Patel, J. J. Lee, Y. Chang, T. J. Kim, J. E. Bae, K. S. Chae and G. H. Lee, *ACS Appl. Mater. Interfaces*, 2010, **2**, 2949-2955.

S13 B. Y. W. Hsu, M. Ng, Y. Zhang, S. Y. Wong, K. Bhakoo, X. Li and J. Wang, *Adv. Funct. Mater.*, 2015, **25**, 5269-5276.

S14 H. Zhang, Y. Ren, F. Cao, J. Chen, C. Chen, J. Chang, L. Hou and Z. Zhang, *ACS Appl. Mater. Interfaces*, 2019, **11**, 29641-29654.

S15 A. Wang, M. Guo, N. Wang, J. Zhao, W. Qi, F. Muhammad, L. Chen, Y. Guo, N.-T. Nguyen and G. Zhu, *Nanoscale*, 2014, **6**, 5270-5278.

S16 J. Xiao, X. M. Tian, C. Yang, P. Liu, N. Q. Luo, Y. Liang, H. B. Li, D. H. Chen, C. X. Wang, L. Li and G. W. Yang, *Sci. Rep.*, 2013, **3**, 3424.

S17 Y. Chen, Q. Yin, X. Ji, S. Zhang, H. Chen, Y. Zheng, Y. Sun, H. Qu, Z. Wang, Y. Li, X. Wang, K. Zhang, L. Zhang and J. Shi, *Biomaterials*, 2012, **33**, 7126-7137.

S18 C.-C. Huang, N.-H. Khu and C.-S. Yeh, *Biomaterials*, 2010, **31**, 4073-4078.

S19 J. Shin, R. M. Anisur, M. K. Ko, G. H. Im, J. H. Lee and I. S. Lee, *Angew. Chem., Int. Ed.*, 2009, **48**, 321-324.

S20 Y. Chen, D. Ye, M. Wu, H. Chen, L. Zhang, J. Shi and L. Wang, *Adv. Mater.*, 2014, **26**, 7019-7026.

S21 Z. Zhao, H. Fan, G. Zhou, H. Bai, H. Liang, R. Wang, X. Zhang and W. Tan, *J. Am. Chem. Soc.*, 2014, **136**, 11220-11223.

S22 L.-S. Lin, J. Song, L. Song, K. Ke, Y. Liu, Z. Zhou, Z. Shen, J. Li, Z. Yang, W. Tang, G. Niu, H.-H. Yang and X. Chen, *Angew. Chem., Int. Ed.*, 2018, **57**, 4902-4906.

S23 W. Zhu, Z. Dong, T. Fu, J. Liu, Q. Chen, Y. Li, R. Zhu, L. Xu and Z. Liu, *Adv. Funct. Mater.*, 2016, **26**, 5490-5498.

S24 G. Yang, L. Xu, Y. Chao, J. Xu, X. Sun, Y. Wu, R. Peng and Z. Liu, *Nat. Commun.*, 2017, **8**, 902.

S25 B. Ding, S. Shao, F. Jiang, P. Dang, C. Sun, S. Huang, P. Ma, D. Jin, A. A. A. Kheraif and J. Lin, *Chem. Mater.*, 2019, **31**, 2651-2660.

S26 Q. Sun, Z. Wang, B. Liu, T. Jia, C. Wang, D. Yang, F. He, S. Gai and P. Yang, *Chem. Eng. J.*, 2020, **390**, 124624.

S27 G. Liang, J. Ronald, Y. Chen, D. Ye, P. Pandit, M. L. Ma, B. Rutt and J. Rao, *Angew. Chem., Int. Ed.*, 2011, **50**, 6283-6286.

S28 D. Ye, P. Pandit, P. Kempen, J. Lin, L. Xiong, R. Sinclair, B. Rutt and J. Rao, *Bioconjugate Chem.*, 2014, **25**, 1526-1536.

S29 D. Ye, A. J. Shuhendler, P. Pandit, K. D. Brewer, S. S. Tee, L. Cui, G. Tikhomirov, B. Rutt and J. Rao, *Chem. Sci.*, 2014, **5**, 3845-3852.

S30 R. Yan, Y. Hu, F. Liu, S. Wei, D. Fang, A. J. Shuhendler, H. Liu, H.-Y. Chen and D. Ye, *J. Am. Chem. Soc.*, 2019, **141**, 10331-10341.

S31 R. An, X. Cheng, S. Wei, Y. Hu, Y. Sun, Z. Huang, H.-Y. Chen and D. Ye, *Angew. Chem., Int. Ed.*, 2020, **59**, 20636-20644.

S32 Y. Hu, J. Zhang, Y. Miao, X. Wen, J. Wang, Y. Sun, Y. Chen, J. Lin, L. Qiu, K. Guo, H.-Y. Chen and D. Ye, *Angew. Chem., Int. Ed.*, 2021, **60**, 18082-18093.

S33 L. Yang, X. Hou, Y. Zhang, D. Wang, J. Liu, F. Huang and J. Liu, *J. Control. Release*, 2021, **339**, 114-129.

S34 X. Liu, N. Xu, X. Pu, J. Wang, X. Liao, Z. Huang and G. Yin, *J. Mater. Chem. B*, 2022, **10**, 4605-4614.

S35 J. Zhang, K. Zhang, Y. Hao, H. Yang, J. Wang, Y. Zhang, W. Zhao, S. Ma and C. Mao, *J. Colloid Interf. Sci.*, 2023, **633**, 679-691.

S36 Q. You, Q. Sun, M. Yu, J. Wang, S. Wang, L. Liu, Y. Cheng, Y. Wang, Y. Song, F. Tan and N. Li, *ACS Appl. Mater. Interfaces*, 2017, **9**, 40017-40030.